Applied Surface Science 401 (2017) 362–372

Contents lists available at ScienceDirect

Applied Surface Science

journal homepage: www.elsevier.com/locate/apsusc

Full Length Article

Functional regulation of Pb-Ti/MoS_2 composite coatings for environmentally adaptive solid lubrication

Siming Ren[a,c], Hao Li[b], Mingjun Cui[a,c], Liping Wang[a,*], Jibin Pu[a,*]

[a] Key Laboratory of Marine Materials and Related Technologies, Key Laboratory of Marine Materials and Protective Technologies of Zhejiang Province, Ningbo Institute of Materials Technology and Engineering, Chinese Academy of Sciences, Ningbo 315201, China
[b] Key Laboratory of Advanced Technologies of Materials (Ministry of Education), School of Materials Science and Engineering, Southwest Jiaotong University, Chengdu 610031, China
[c] University of Chinese Academy of Sciences, Beijing 100039, China

ARTICLE INFO

Article history:
Received 30 September 2016
Received in revised form
24 December 2016
Accepted 6 January 2017
Available online 8 January 2017

Keywords:
Humid environment
Pb-Ti/MoS_2 composite coatings
Ultra-low friction coefficient
H/E ratio

ABSTRACT

The lubrication of molybdenum disulfide coatings has commonly been limited by the application environments, for instance, the crystal MoS_2 are easily affected by water to form MoO_3 that causes a higher friction coefficient and short lifetime. Therefore, to improve the tribolgical performance of MoS_2 in high humidity condition, the co-doped Pb-Ti/MoS_2 composite coatings are deposited by unbalanced magnetron sputtering system. The design of the co-doping elements in MoS_2-based coatings can not only maintain the characteristic of low humidity-sensitivity as the Ti/MoS_2 coating but also improve the mechanical properties and tribological performance of coatings as a comparison with single-doped ones. Moreover, the ultra-low friction coefficient with a minimum value of 0.006 under the vacuum condition is achieved for Pb-Ti/MoS_2 composite coating containing about 4.6 at.% Pb, depending on the densification structure of coating. Intriguingly, the wear behaviours of Pb-Ti/MoS_2 composite coatings are in accordance with the variation in *H/E* (hardness to the elastic modulus) ratio that the coating with higher *H/E* exhibits lower wear rate. These results demonstrate that the lubricating properties of MoS_2 coatings in both humid environment and vacuum condition can be achieved through the Pb and Ti co-doped, which is of great significant for developing MoS_2 coatings as the environmentally adaptive lubricants.

1. Introduction

The tribological properties of solid lubricant coatings based on the transition metal dichalcogenides (TMD-sulfides) are of technological interest for reducing friction in circumstances where liquid lubricants are impractical [1–3]. The low friction of TMDs derives from the weak interatomic interactions between their layered structures, resulting in very low strength shearing [4,5]. MoS_2, as the most abundant TMD, has been widely used in various applications on earth and space such as main weather sensor bearings, release mechanisms, precision bearing applications, and many others [6,7]. Unfortunately, when the S-Mo-S planes are oriented perpendicular to the substrate, the exposed edges of these basal planes are easily oxidized by water molecular and oxygen which may deteriorate the sliding properties [8,9]. Therefore, improving the tribological performance of MoS_2-based coatings is an increasing demand for environmentally robust solid lubricant coatings. In general, the space components are often exposed in moist environment for a period of time during the moving mechanical assemblies (especially for the coastal launch site) [10].

Controlling the deposition parameters is an effective method to improve the lifetime of MoS_2 coating in humid environments [11]. Researchers found that coating with basal plane orientation (002) parallel to substrate had a best tribological performance than that with other orientations [12–14]. Moreover, *basal-oriented* coatings are denser than *random-oriented* ones which can enhance the oxidation resistance of coating in humid [14]. However, this orientation is obtained only in a few cases since most deposition processes results in a random orientation [15,16]. In the past two decades, metal dopants in MoS_2 had been studied and reported, which could increase the densification of coating and consequently reduce porosity columnar structure. At the meantime, the hardness, adhesion strength and tribological performance of the composite coatings were also improved significantly in air over the pure MoS_2 coating. Among many metals used for alloying (Ti [6,17,18], Pb

* Corresponding authors.
E-mail addresses: wangliping@nimte.ac.cn (L. Wang), pujibin@nimte.ac.cn (J. Pu).

http://dx.doi.org/10.1016/j.apsusc.2017.01.054
0169-4332/

Table 1
Parameters for deposition process of the composite Pb-Ti/MoS_2 coatings.

Run No.	1	2	3	4	5	6
Magnetron current (A), MoS_2	0.8					
Magnetron current (A), Ti	0.2					
Magnetron current (A), Pb	0	0.1	0.2	0.3	0.4	0.5

[19–21], Al [22,23], Au [5,23,24], Cr [25,26]), titanium, as the most potential candidate from the view of commercial application, that added into molybdenum disulphide can increase the hardness and wear resistance of coating and make it less sensitive to humid environments. However, the addition of Ti could not give a contribution for ultra-low friction in vacuum [8]. It is well known that Pb is the promising dopant, which is not only because it is an excellent solid lubricant for space [27], but also because it can facilitate the formation of basally oriented MoS_2 crystallites during wear process to achieve a long endurance of MoS_2 coatings [20,28]. Until now the synergistic effect of co-doped Pb-Ti metals with MoS_2 coating was still not reported in the literature.

In this study, a series of Pb-Ti/MoS_2 composite coatings were deposited using unbalanced magnetron sputtering system. According to previous researches [29,30], it could be found that the MoS_2 coating with low content of Ti exhibited enhanced mechanical properties than pure MoS_2 coating, whereas MoS_2 coating with high content of Ti presented high friction coefficient in air and short wear life in vacuum. Hence, a constant target current for low content of Ti and varying target current for different content of Pb were controlled during the deposition process. Unlike results obtained in Ti/MoS_2 or Pb/MoS_2 coating, the co-doped Pb-Ti/MoS_2 composite coatings showed lower friction coefficient and longer wear life in both humid and vacuum environments than that of single-doped ones. The major objective of this study was to investigate the effect of Pb-Ti co-doping elements on the microstructure, mechanical properties and tribological performance of the coating. Additionally, the friction and wear mechanism of Pb-Ti/MoS_2 composite coatings in both humid and vacuum environments were also discussed systematically.

2. Experimental details

2.1. Deposition of the Pb-Ti/MoS_2 composite coatings

A series of Pb-Ti/MoS_2 composite coatings with different Pb contents were deposited on 304 stainless steel and silicon wafer synchronously by a Teer UDP-650 unbalanced magnetron sputtering system. The sputtering system was combined with one Ti target, one Pb target and two molybdenum disulphide compound targets. All the targets were sputtered with direct current (DC) power. The substrates were first cleaned ultrasonically in acetone and alcohol bath for 20 min, respectively, and then dried in nitrogen. Prior to the coating deposition, the substrates were etched by Ar^+ ions in a vacuum chamber to remove the surface contaminations. Subsequently, a titanium intermediate layer with a thickness about 0.2 μm was deposited on the substrate to improve the adhesion between the coating and substrate. The final step was deposition of the main bulk of composite Pb-Ti/MoS_2 coatings. During the deposition process, control of the coating composition was achieved by applying a constant DC power density on the Ti and MoS_2 targets and tuning the power density on the Pb target. The samples were denoted as Run No. 1–6 coatings (Run No. 1 coating corresponding to the Ti/MoS_2, and Run No. 2–6 coatings corresponding to the Pb-Ti/MoS_2 coatings with various target current of Pb, respectively). Detailed parameters for deposition process of the composite Pb-Ti/MoS_2 coatings were summarized in Table 1.

2.2. General characterization

Atomic force microscopy (AFM, Benyuan CSPM 4000) with contact mode was used to measure the surface roughness of the Pb-Ti/MoS_2 composite coatings. The cross-sectional micrographs of the Pb-Ti/MoS_2 composite coatings were observed by field emission scanning electron microscopy (FESEM, Hitachis-4800). The composition and chemical bonds of the deposited coatings were analysed by X-ray photoelectron spectroscopy (XPS, Axis ultra DLD) with Al (mono) Kα irradiation at the pass energy of 160 eV. Before taking the measurement, an Ar^+ ion beam with the energy of 3 keV was used to each the sample surface for 5 min to remove contaminants. The structure of the coatings was measured by a Philips X'perts X-ray diffractometer with Cu Kα radiation and the scanning was range from 5° to 75°. Further investigation of the microstructure characterization was performed via transmission electron microscopy (TEM) and high-resolution TEM (HRTEM) using Tecnai F20 operated at 300 kV. The lamella of sample was prepared by using a focused ion beam (FIB, Auriga, Germany), followed by a short ion-beam thinning using the precision ion polishing system (PIPS) of Gatan. The nanohardness (H) and Young's modulus (E) of as-deposited coatings were measured using a Nanoindenter (MTS NanoIndenter G200) with a diamond Berkovich (three-sided pyramid) indenter tip, and the indentation depth was about 200 nm (less than 10% of the coating thickness to minimize the substrate contribution). The indentations of each coating specimen were measured for five measurements to calculate the average value.

2.3. Tribological experiment

The tribological behaviour of the Ti/MoS_2 and Pb-Ti/MoS_2 composite coatings under atmosphere condition was investigated by a ball-on-disc reciprocating sliding tribometer (CSM, Tribo-*S*-D-0000). The humidity was fixed at 75 ± 3% RH. Friction tests were performed at a constant load of 5 N, the reciprocating amplitude was 5 mm, and the sliding frequency was 5 Hz. The total reciprocating test duration was 20,000 cycles. The counterpart was a GCr15 ball with a diameter of 4 mm and the hardness of 6.1 GPa. The tribological performance in vacuum was evaluated by a Bainano rotational ball-on-disc vacuum tribometer. The normal load of 5N was applied through a stationary loading system. The rotate radius was 10 mm at 600 rotations per minute (rpm) and the total rotation sliding cycle number was 20,000 cycles. The tribopair was identical to the atmosphere condition. All the friction tests were carried out at room temperature and the vacuum chamber pressure was less than 1.0×10^{-3} Pa. The friction coefficient was continuously recorded during testing. After friction test, the depth of wear track was measured using a surface profiler (Alpha-step D-100). The wear volume of each wear track was calculated for three to five measurements to obtain the average value. The wear rates of the coatings were calculated from their wear volumes using the following equation:

$$K = V/SF \quad (1)$$

where V is the wear volume in stere, S is the total sliding distance in meter, and F is the normal load in newtons.

3. Results and discussion

3.1. Composition and microstructure

The compositions of as-deposited Ti/MoS_2 and Pb-Ti/MoS_2 composite coatings are analysed by XPS, as shown in Table 2. The content of Ti ranges from 2.0 to 2.9 at.% because of the constant target current during deposition process (0.2 A). The Pb content

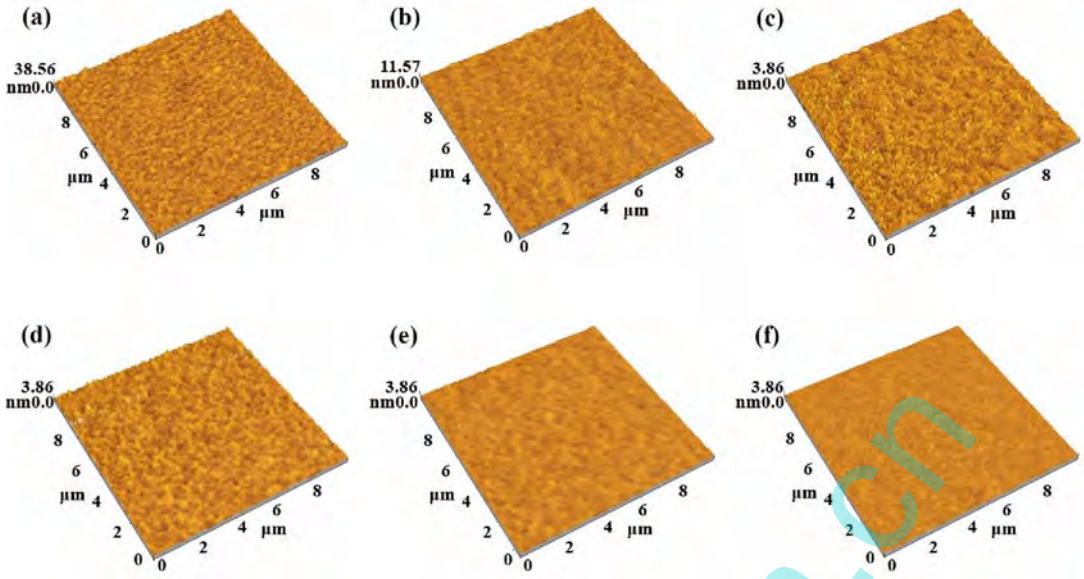

Fig. 1. AFM morphologies of Ti/MoS_2 (a), and Pb-Ti/MoS_2 composite coatings with Pb content of 1.7 (b), 4.6 (c), 6.3 (d), 6.8 (e), and 8.7 at.% (f).

Table 2
The elemental content and surface roughness of the Pb-Ti/MoS_2 composite coatings.

Run No.	1	2	3	4	5	6
S%	51.5	49.8	51.2	49.4	49.8	48.8
Mo%	37.6	37.2	34.1	34.8	35.5	36.0
Ti%	2.0	2.6	2.9	2.9	2.6	2.4
Pb%	0	1.7	4.6	6.3	6.8	8.7
O%	8.9	8.7	7.2	6.6	5.3	4.1
S/Mo	1.37	1.34	1.50	1.42	1.40	1.36
R_a/nm	2.75	0.63	0.33	0.25	0.13	0.12

increases from 0 to 8.7 at.% with the increase in the target current of Pb. The change of S/Mo ratio (the atomic percent of S to Mo) is not obvious and the value of ratio is lower than that of MoS_2 stoichiometric, regardless of the variation of Pb content. The relative low S/Mo ratio of as-deposited coating is due to the S is easier to sputter out of the surface than Mo during deposition of the coating [31]. The AFM surface morphologies of the Ti/MoS_2 and Pb-Ti/MoS_2 composite coatings are presented in Fig. 1. It is found that the surface morphologies and roughness of the as-deposited composite coatings are obviously different. Moreover, the surface of coatings is composed of small spheres which size decreases with the increase in the Pb content. The concrete value of surface roughness is shown in Table 2. Compared with the roughness value of the Ti/MoS_2 coating (R_a = 2.75 nm), the roughness of Pb-Ti/MoS_2 composite coatings decreases dramatically. When the Pb content rises to 8.7 at.%, the coating has a flat texture and the value of R_a is only 0.12 nm. Therefore, it can be concluded that the Pb-doping probably caused reduction of the roughness of MoS_2 coatings.

The cross-sectional images of as-deposited Ti/MoS_2 and Pb-Ti/MoS_2 composite coatings by FESEM are illustrated in Fig. 2. The total film thickness ranges from 2.2 to 2.6 μm, which is attributed to the discrepancy of deposition rates. The Ti/MoS_2 coating reveals a typical porous with columnar structure as shown in Fig. 2(a), whereas the Pb-Ti/MoS_2 composite coatings (Fig. 2b–f) show a dense and featureless microstructure even when the Pb content is as low as 1.7 at.% (Run No. 2 coating). This is probably because the doping Pb disrupted the MoS_2 crystallite growth and the resulting coatings are typically amorphous [19]. Moreover, the amorphous structure does not change obviously with the variation of Pb content.

The chemical bonds of the deposited Ti/MoS_2 and Pb-Ti/MoS_2 composite coatings with different Pb contents are characterized by XPS spectrum as shown in Fig. 3. The peaks shapes of all samples are very similar to each other, which indicate the chemical bonds of mainly containing elements of coatings don't change obviously. Interestingly, the intensity of Pb 4d spectrum for Run No. 6 coating is higher than that of No.2 ones which implies higher content of Pb. In order to further justify the chemical forms of Mo, S and Pb in the coatings, the Mo 3d, S 2p and Pb 4f spectrum of the typical coating with the Pb content at 6.3 at.% is fitted by Guassian-Lorentian function, as shown in Fig. 4. The Mo 3d spectrum for all the samples with a small hump at around 226.0 eV is identified as the S 2s peak [32]. The Mo 3d peak at binding energy of 228.8 and 231.9 eV corresponds to Mo^{4+} ions like those present in MoS_2, whereas the Mo 3d peak at 235.0 eV assigned to MoO_3 is hardly detected [28,32–34]. This suggests that Mo in the bulk of coating is less influenced by oxygen. Moreover, there is another Mo 3d doublet in the deconvolution of the Mo 3d spectrum shown in Fig. 4a. The peaks at 228.1 and 231.2 eV are consistent with the Mo 3d5/2 and Mo 3d3/2 in MoS_{2-x}, respectively, which can be explain why the ratio of S to Mo is lower than 2 (about 1.34–1.50) [32–34]. The S 2p spectrum (Fig. 4b) shows a doublet at 162.4 and 163.6 eV, which represents the S 2p3/2 and S 2p1/2 spectral lines of S^{2-} in MoS_2. And the deconvolution of S 2p peaks at 161.6 and 162.8 eV corresponds to the standard S 2p3/2 and S 2p1/2 lines of S^{x-2}, which is in good agreement with the analysis of Mo 3d spectrum [32–34]. For the Pb 4f spectrum (Fig. 4c), the Pb 4f7/2 peak at 136.9 and 138.2 eV is assigned to Pb and PbO_x, respectively, indicating that part of Pb in the coating is oxidized [28,34,35]. However, for the Ti 2p spectrum, it is difficult to distinguish the chemical state by Guassian-Lorentian due to its low content and high interference signal. Fortunately, as shows in Fig. 3, the weak peak of Ti 2p3/2 at about 454.1 and 458.8 eV is assigned to Ti and TiO_x, indicating Ti element mainly exists in the form of metallic Ti and oxidized Ti [32,34]. Therefore, Pb-Ti/MoS_2 composite coatings are mainly composed of MoS_2, metallic Pb and Ti, and part of Pb and Ti are oxidized during deposition. Oxidation of MoS_2 is reduced to a great extent owing to the existence of Pb and Ti.

The structures of the as-prepared coatings are checked by XRD and HRTEM. Fig. 5 shows the evolution of crystallinity of the as-deposited coatings as a function of the Pb content measured by the

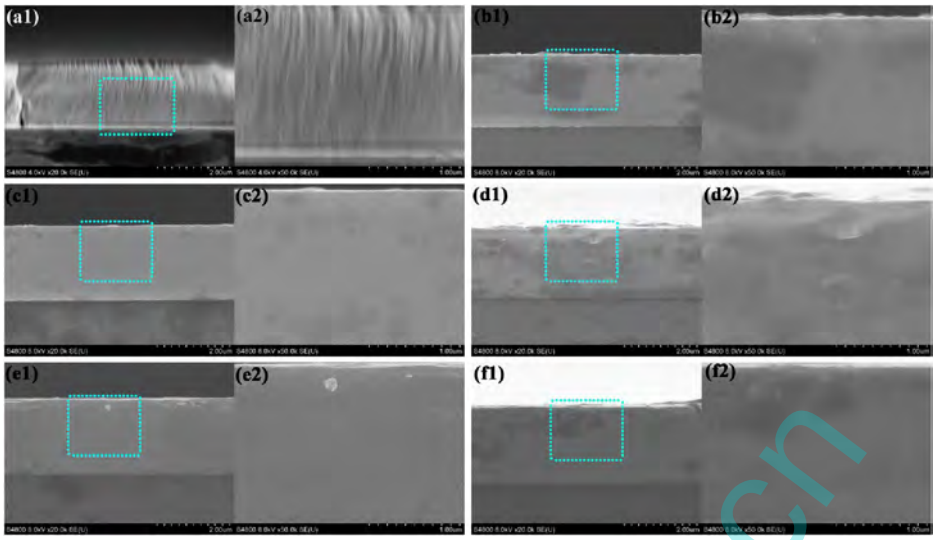

Fig. 2. Cross-sectional SEM micrographs of Ti/MoS_2 (a), and Pb-Ti/MoS_2 composite coatings with Pb content of 1.7 (b), 4.6 (c), 6.3 (d), 6.8 (e), and 8.7 at.% (f). Magnified images of (a2-f2) are corresponding selected region of (a1-f1).

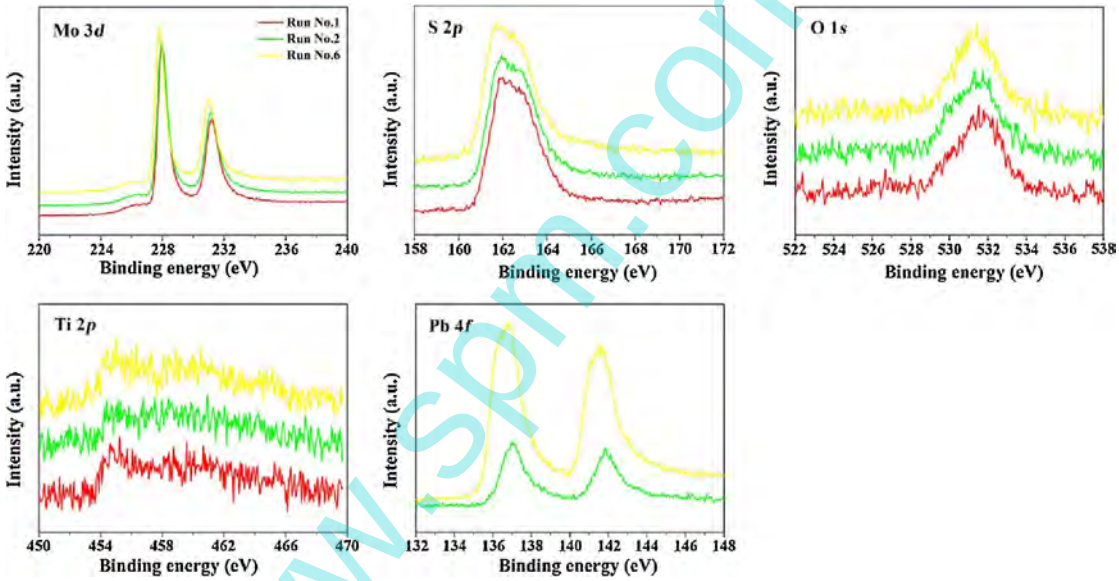

Fig. 3. XPS spectrum of Mo 3d, S 2p, O 1s, Ti 2p and Pb 4f measured after Ar+ etching.

XRD spectra. Results manifest that the Ti/MoS_2 coating has a typical crystalline nature with crystals oriented mostly in the (002) plane of MoS_2 (Fig. 3a), which is assigned to diffraction peak at around $2\theta = 13^\circ$. The weak peak at around $2\theta = 33^\circ$ is ascribed to the MoS_2 (100) plane. These results indicate that Ti/MoS_2 coating with its basal planes are mainly oriented parallel to the substrate, which has a similar structure to the pure MoS_2 [32]. In general, MoS_2 (100) plane reflection predominate because the crystals within the coating are preferentially oriented with these planes perpendicular to the substrate surface, while the (002) plane orientates parallel to substrate surface [36]. More importantly, coatings with basal planes oriented parallel to the substrate surface are more resistant to oxidation and can lead to low values of friction coefficient. However, the (100) plane disappear when Pb is incorporated into Ti/MoS_2 coating. The presence of Pb leads to re-arrangement of the deposited MoS_2 and the formation of the nucleation sites favouring basal crystalline growth [28]. Moreover, with the increasing of Pb component, the intensity of (002) peak is weakened and the FWHM (full widths at half maximum) increased. It is well know that disorder can produce a broadening of X-ray reflections and, in layered structures, an increase of the interlayer distance along the c-axis. While doping of Ti and Pb with layered structure of MoS_2 forms a random modulation between the layers and these layers rotate and tilt, causing distortion [37]. When the Pb content rises to 6.3 at.% (Run No. 4 coating), the (002) peak disappears and no other peaks related to the Pb-Ti/MoS_2 composite coatings can be observed, implying that the Pb-Ti/MoS_2 composite coating is possible dominated by amorphous structure. Actually, the general features observed in the present XRD patterns can be ascribed to disorder effects induce by the Ti and Pb incorporation. Moreover, no diffraction peaks of Ti and Pb can be found in the XRD patterns. It is inferred that the doping elements of Ti and Pb mainly exist in the coatings by the amorphous types or nanocrystalline. At the same time, the Raman spectra of Ti/MoS_2 and Pb-Ti/MoS_2 composite coatings are carried out to verify the variation of structure with the increasing of Pb content. As shown in Fig. 6, two peaks of TMD (around 400 cm^{-1}) are observed with the Run No. 1 and No. 2 sample, however, no distinct MoS_2 peaks are observed with the

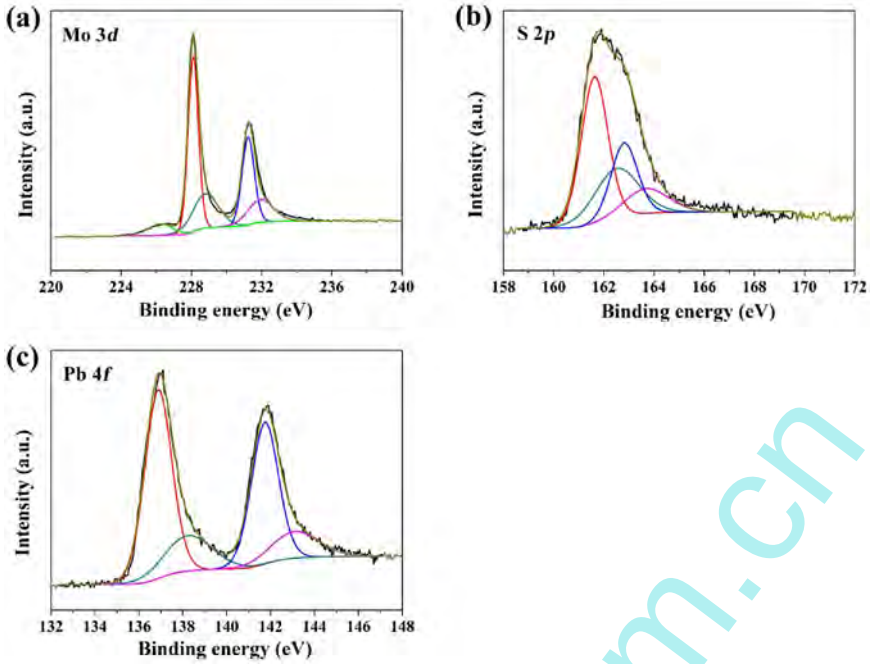

Fig. 4. Decomposition of Mo 3d (a), S 2p (b) and Pb 4f (c) spectral regions of the typical coating with the 6.3 at.% Pb.

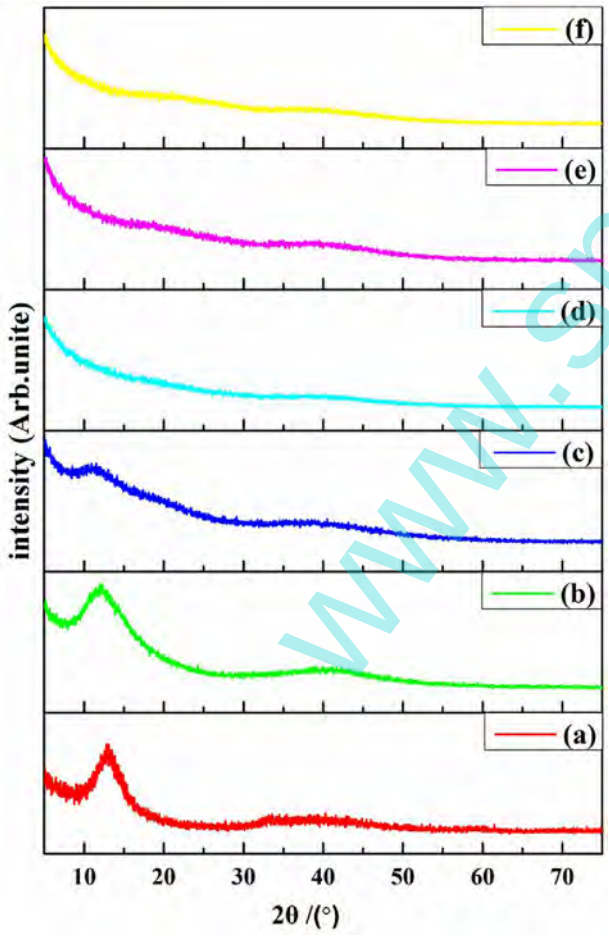

Fig. 5. XRD patterns of Ti/MoS_2 (a), and Pb-Ti/MoS_2 composite coatings with Pb content of 1.7 (b), 4.6 (c), 6.3 (d), 6.8 (e), and 8.7 at.% (f).

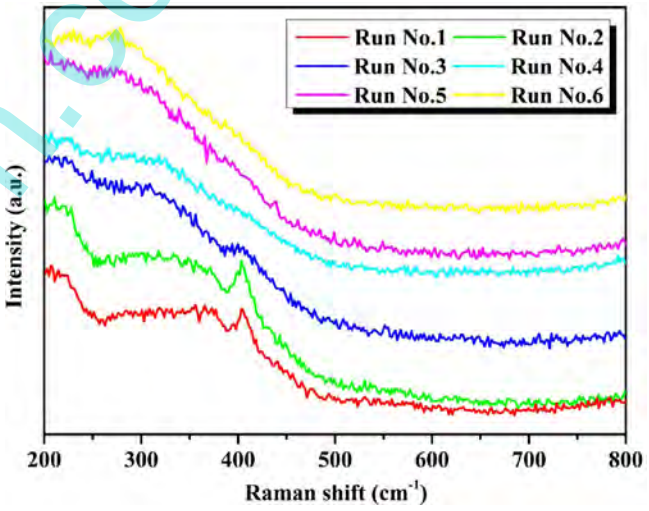

Fig. 6. Raman spectra of (a) Ti/MoS_2, and Pb-Ti/MoS_2 composite coatings with Pb content of 1.7 (b), 4.6 (c), 6.3 (d), 6.8 (e), and 8.7 at.% (f).

Run No. 3 to No. 6 coatings. According to the literature reports, two well-defined bands appeared at 383 (E_{2g}) and 408 cm^{-1} (A_{1g}) in Raman spectra are in correspondence with the single crystal data [38,39]. E_{2g} and A_{1g} are two signature bands of MoS_2 crystals and thus represent the bonding condition between Mo and S atoms within the lattice. The changing of the E_{2g} and A_{1g} peaks for the Run No. 1 and No. 2 coatings is attributed to the incorporation of Ti and Pb into the MoS_2 crystal lattice, which subsequently altered the interatomic vibration mode between Mo and S [39]. Notably, the decreasing Raman signal of MoS_2 with increase in Pb content is owing to shielding from the composite structure [39]. Based on the XRD and Raman results, we can safety conclude that the crystallization of Pb-Ti/MoS_2 composite coatings decreases with the increasing Pb content and the structure of coatings appears to be amorphous when Pb content rises to 6.3 at.%, which is consistent with previous publications on these materials [29].

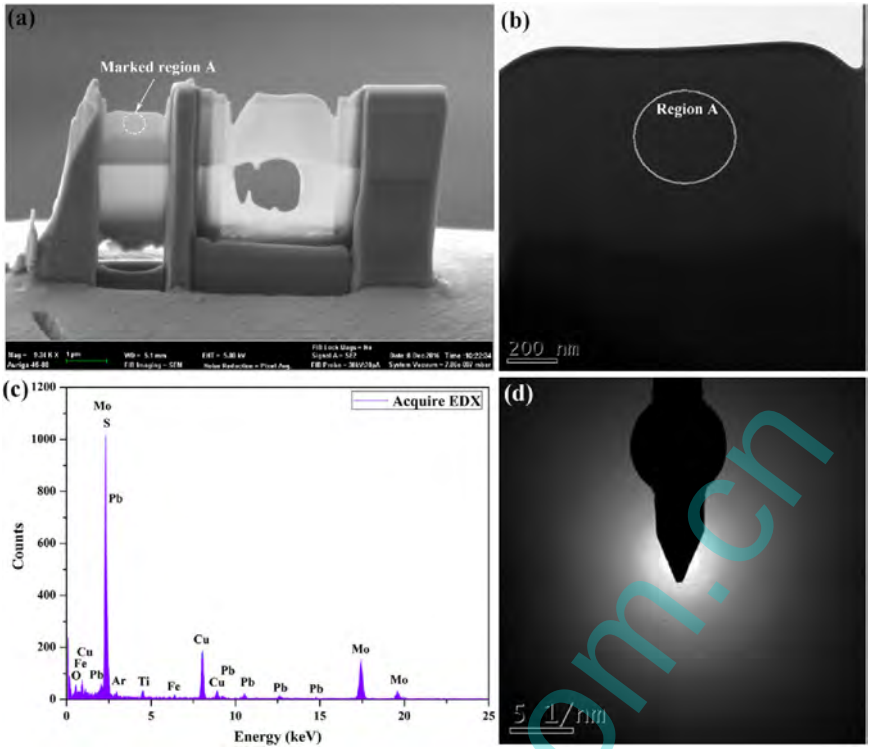

Fig. 7. TEM-FIB lamella (a) and (b) microstructure of Pb-Ti/MoS_2 composite coating with Pb content of 6.3 at.%. (c) EDX and (d) SAED patterns taken from the marked region A in Fig. 5a and b.

Transmission electron microscopy (TEM) images and corresponding selective area electron diffraction (SAED) patterns are used to further evidence the morphologies and crystal structures of Pb-Ti/MoS_2 composite coating. Fig. 7 shows the cross-sectional TEM micrograph taken from FIB lamella and corresponding selected area EDX as well as selected area electron diffraction (SAED) pattern of the coating with 6.3 at.% Pb. EDX analysis (Fig. 7c) of the marked region A (Fig. 7b) indicates the presence of Mo, S, Pb, Ti and small amounts of O. The SAED shows the broad and diffuse halo diffraction (Fig. 7d), which is the typical amorphous feature. This result is in correspondence with the XRD observation (Fig. 5).

A cross-sectional TEM micrograph of the Pb-Ti/MoS_2 composite coating with Pb content of 6.3 at.% obtained from TEM-FIB lamella is shown in Fig. 8a, which includes Si wafer substrate, Ti intermediate layer and Pb-Ti/MoS_2 layer. The intermediate Ti layer displays a crystalline structure (Fig. 8c, I), while Pb-Ti/MoS_2 layer (coating layer) appears amorphous with bright and dark stripes (Fig. 8c, III). It supports the theory that Pb nanocrystalline formed during deposition of the Pb-Ti/MoS_2 coating can promote the amorphous structure and prevent the formation of a layered arrangement, thus resulting in a denser structure than that of Run No. 1 coating. Interestingly, some amorphous phase is also found in the areas of the intermediate layer close to the coating (Fig. 8c, II), which is related to the diffusion of coating elements to Ti intermediate layer. Here the coating layer shows a disordered layered structure and a wavy-like morphology (Fig. 8b and d). The long-range order of pure MoS_2 coating reported in literature is reduced when Pb and Ti atoms are introduced into the lattice [40]. This disordered atomic arrangement is a clear indication to explain why the reflection peak of MoS_2 (200) at 13° in Pb-Ti/MoS_2 coating is disappeared (Fig. 5). The crystalline structure of the Pb-Ti/MoS_2 composite coating is further observed using HRTEM, as shown in Fig. 8e and f. The HRTEM image reveals that the nanocrystalline particles of Pb and Ti co-exist in the coating and the orientation of crystals separated irregularly (as indicated by the arrow, Fig. 8e). Numerous short black lines with an interplanar spacing about 0.65 nm are assigned to MoS_2 clusters [41]. Meantime, an interplanar spacing measurement for particular nanocrystals reveals that Ti and Pb nanocrystals with a size of 2–5 nm (Fig. 8e and f) are also present in the coating. It confirms that the presence of nanocrystalline particles of Pb and Ti hampers the growth of the MoS_2 crystal and causes the re-arrangement of MoS_2 crystals [42]. As a result, the amorphous structure of Pb-Ti/MoS_2 coating is derived from the re-arrangement of MoS_2 crystals, which is in consistency with the XRD and Raman results.

3.2. Mechanical properties

The mechanical properties of the MoS_2-based coatings are strongly affected by the introduction of metallic Ti and Pb. The main results for the hardness (H) and elastic modulus (E) of Ti/MoS_2 and Pb-Ti/MoS_2 composite coatings are displayed in Fig. 9. It can be seen that the co-doped composite coatings show significantly higher hardness and elastic modulus than Ti/MoS_2 coating. Especially for the low level of dopant (1.7 at.% Pb), the hardness increases from ~5.1 GPa for the Ti/MoS_2 coating to ~7.2 GPa for the Pb-Ti/MoS_2 composite coating and the Young's modulus also increases from ~77 GPa to ~97 GPa. This lower hardness and elastic modulus for the Ti/MoS_2 coating can be related to its highly columnar morphology with large crystallites not strongly bonded [43]. In contrast, the introduction of Pb nanocrystalline in Ti/MoS_2 matrix may cause the distortion of the MoS_2 lattice to block the columnar crystal growth, thus leading to a denser coating structure [26]. It is a fact that the densification structure of Pb-Ti/MoS_2 composite coatings is responsible for the hardness and elastic modulus enhancement. As the Pb content increases from 1.7 to 8.7 at.%, the hardness of Pb-Ti/MoS_2 composite coatings decreases gradually from 7.2 to 6.3 GPa. The same tendency is also observed in elastic modulus that dropped from 97 GPa for 1.7 at.% Pb to 84 GPa for 8.7 at.% Pb, which is mainly attributed to the grain boundary sliding. Based on the AFM results (Fig. 1), the roughness and crystalline size decrease with

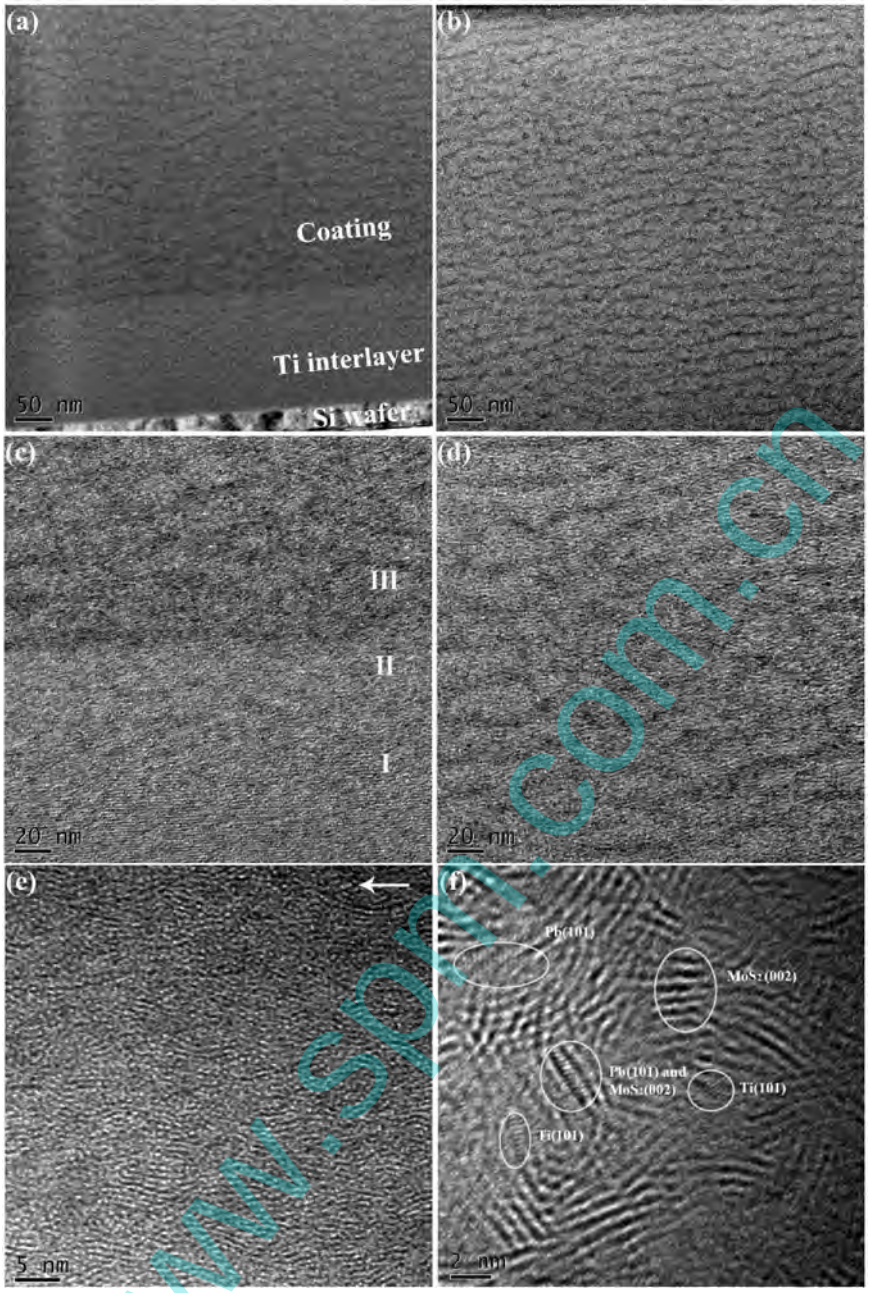

Fig. 8. Cross-sectional TEM micrograph of the coating-substrate interface region (a) and intermediate layer-coating layer interface region (c), coating region with different magnifications (b, d) and HRTEM details of the coating (e, f).

the increase in Pb content, indicating the grain boundary increases rapidly. According to the negative Hall-petch relationship, when the crystalline size decreases below a certain limit, the increased grain boundaries can decrease the strength and hardness of coating owing to the phenomenon of grain boundary sliding [44,45]. Another reasonable explanation is that the Pb grains in the coating is easy to deform during external penetration and then the compressive stress of coating is relaxed owing to the deformation, which results in the decreasing hardness of coating [28,46].

3.3. Tribological properties

To investigate the effect of co-doped metallic elements (Pb-Ti) and the Pb content on the tribological behaviours of MoS_2-based coatings, ball-on-disk friction tests are performed under ambient air environment with high relative humidity (75% RH) and vacuum condition. Fig. 10a shows the friction curves of the Ti/MoS_2 and Pb-Ti/MoS_2 composite coatings against the GCr15 steel ball as a function of sliding cycle in 75% RH atmosphere. Results show that the Run No. 1 coating (Ti/MoS_2) has a highest friction coefficient with a value of 0.12 than other Run No. coatings at the stable stage. In the low level of dopant (1.7 at.% Pb), the friction coefficient of composite coating decreases gradually about 0.11. With the further increase of Pb content, the friction coefficient decreases continuously to a minimum value of 0.065 for 6.3 at.% Pb (Run No. 4 coating) and thereafter increases with further increasing the Pb content. However, the Run No. 6 coating still exhibits a lower friction coefficient than that of Run No. 1 ones. It indicates that the co-doped Pb and Ti improve the tribological properties of single-doped ones in the atmospheric environment. Fig. 10b shows the

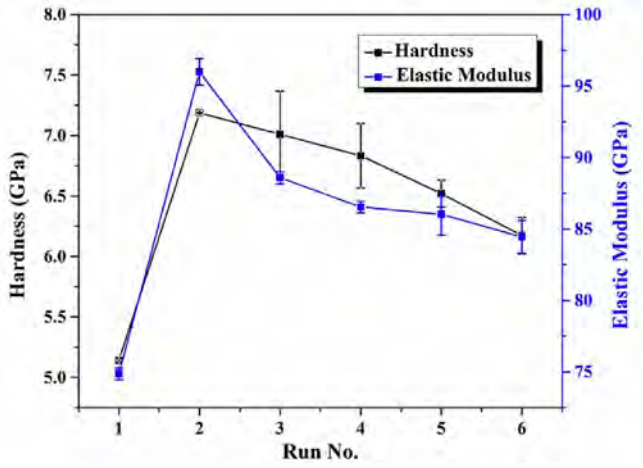

Fig. 9. Hardness and elastic modulus of Ti/MoS_2 and Pb-Ti/MoS_2 composite coatings.

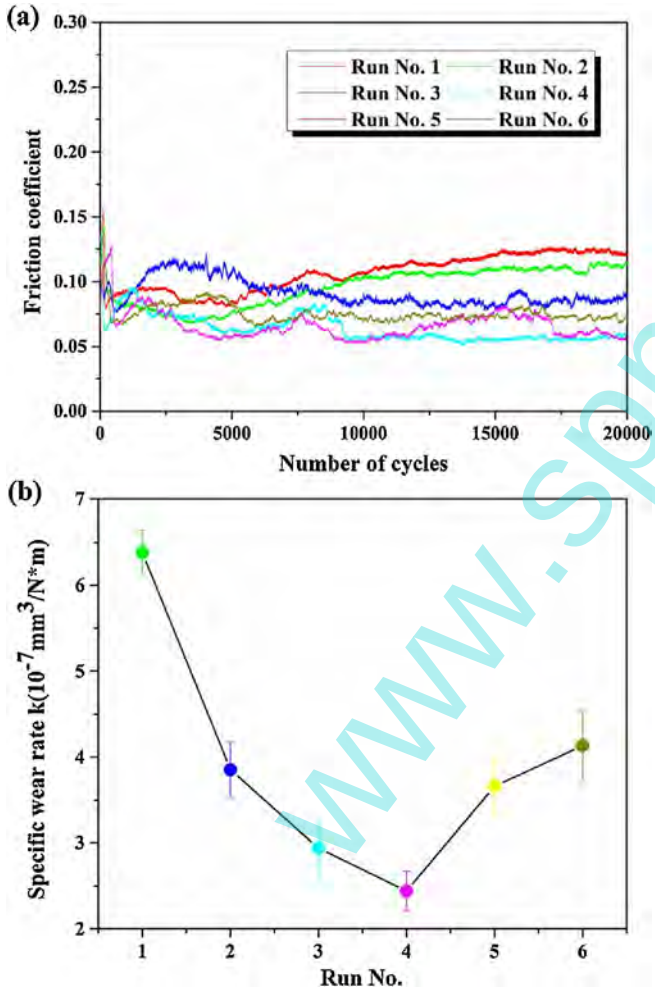

Fig. 10. Sliding friction curves (a) and the corresponding average wear rates (b) of Ti/MoS_2 and Pb-Ti/MoS_2 composite coatings under 75% RH.

average wear rates of the Ti/MoS_2 and Pb-Ti/MoS_2 composite coatings after 20,000 sliding cycles under 75% RH. As shown in Fig. 10b, the wear rates of Ti/MoS_2 and Pb-Ti/MoS_2 composite coatings have a similar tendency to the friction curve (Fig. 10a) that the values of wear rate decrease first and increase afterwards with the increase in Pb content. The Ti/MoS_2 coating presents the highest value of 6.37×10^{-7} mm^3/N.m among all the Run No. coatings. In comparison, the wear rate of Pb-Ti/MoS_2 composite coatings is lower than that Ti/MoS_2 coating, which indicates the Pb nanocrystalline embedded into MoS_2-based matrix is beneficial to decrease the friction and wear of coating. According to the Ref. [26], Ti-doped MoS_2 can improve the oxidation resistance of MoS_2 coating because that Ti element is easy to react with the water molecules and dissolved oxygen and to form a compact protect film that retards oxidation process. Moreover, the incorporation of Pb into the MoS_2-based matrix can enhance the densification of coating, which inhibits the penetration of oxygen and water vapour into the coating and then avoids the oxidation of coating. Therefore, the synergistic effect of co-doped Pb-Ti elements can modify the tribological performance of MoS_2 coating in humid air. Particularly, the lowest wear rate is obtained from the Pb-Ti/MoS_2 composite coating with 6.3 at.% Pb, which confirms that the composite coatings with appropriate Pb content can present excellent tribological performance under high RH.

In order to understand the wear mechanism of the metal-MoS_2 composite coatings in high RH environment, the optical morphologies of worn surface for different Run No. coatings are observed, as shown in Fig. 11. All specimens reveal a smooth and burnished appearance, and the periphery of worn surface is covered with much wear debris powder. For the Ti/MoS_2 coating (Fig. 11a) and coatings with relatively low content of Pb (Fig. 11b), the wear track is relatively wide and accompanied with some shallow grooves along the sliding direction. These are typical features associated with abrasive wear, in which hard particles exists in between the coating and steel ball, causing a high removal of material [47]. With the increase in Pb content, the improved densification of coating leads to the increasing oxidation resistance of coating, thus resulting in the decreasing widths of wear track and reduced groove. However, further increase of the Pb content results in an increase of the groove depth in wear track, which is relate to the declined hardness of coating with the increase in Pb content (Fig. 9).

Fig. 12 shows the friction coefficient and the corresponding average wear rates of Ti/MoS_2 and Pb-Ti/MoS_2 composite coatings against the GCr15 under vacuum condition. As shown in Fig. 12a, the friction coefficient of Ti/MoS_2 coating reaches to a stable level with an average value of 0.029 after 2000 sliding cycles. Moreover, the friction coefficient of Ti/MoS_2 coating is higher than that of other coatings. According to our aforesaid conclusion, the Ti/MoS_2 coating has good oxidation resistance and tribological performance in humid air. Although the friction coefficient of Ti/MoS_2 coatings is lower than that of pure MoS_2 coating (0.040) under vacuum condition, its vacuum tribological performance is limited due to the adhesion effect between the Ti and GCr15 during friction test [30]. Surprisingly, the incorporation of Pb in composite coating can alleviate the adhesion effect and the tribological behaviours in vacuum are improved notably even when the Pb content is less than 1.7 at.%. The friction coefficient decreases from 0.029 for Run No. 1 coating to a minimum level approximately 0.005 for Run No. 3 coating, and then increases to 0.022 when Pb content reaches to 8.7 at.% (Run No. 6 coating). Fig. 12b shows the average wear rates of Ti/MoS_2 and Pb-Ti/MoS_2 composite coatings under vacuum environment after 20,000 sliding cycles. The variation of wear rates for composite coatings is consistent with the corresponding results of friction coefficient: for all samples, the wear rates decrease first and increase afterwards with increasing Pb content. Furthermore, the coating with the appropriate Pb content (Run No. 3 coating, namely 4.6 at.% Pb) exhibits the lowest wear rate. It can be noted that the wear rate of Ti/MoS_2 coating is higher than that of Pb-Ti co-doping coatings, indicating the co-doping elements in MoS_2-based coating can improve the mechanical and tribological performance. So,

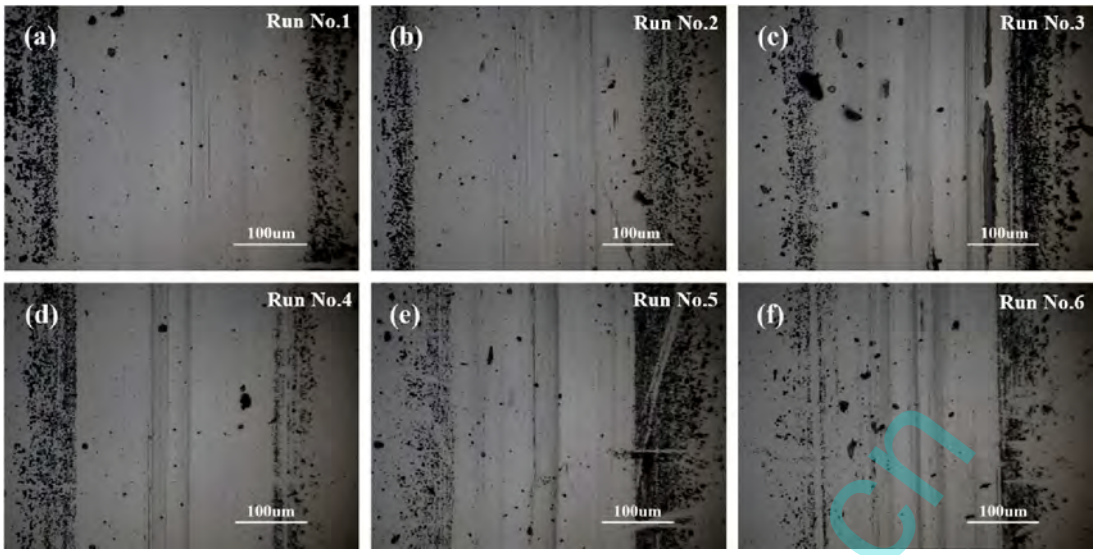

Fig. 11. Optical images of wear tracks of Ti/MoS_2 and Pb-Ti/MoS_2 composite coatings after 20,000 sliding cycles under 75% RH.

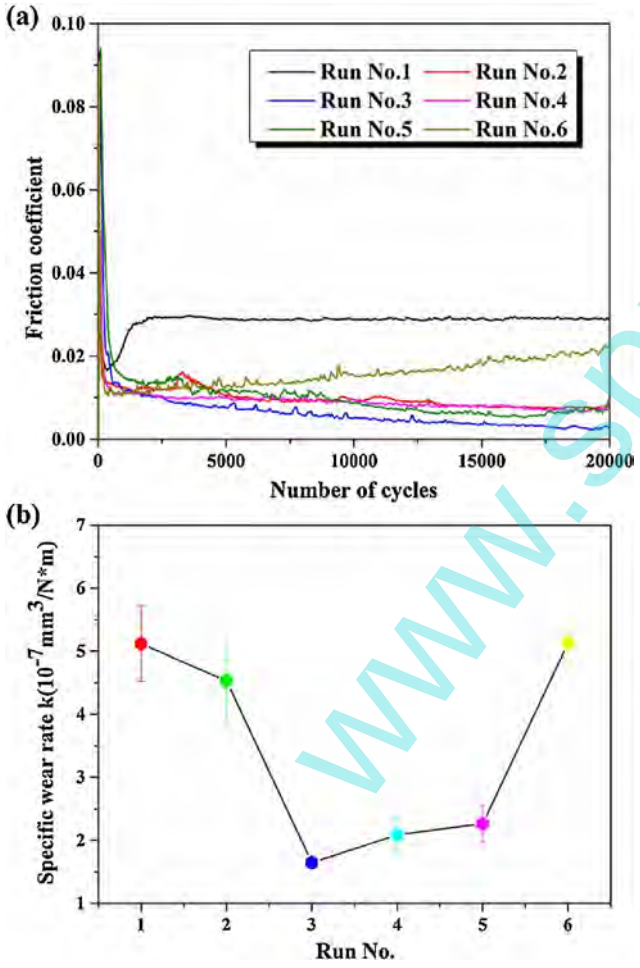

Fig. 12. Sliding friction curves (a) and corresponding average wear rates (b) of Ti/MoS_2 and Pb-Ti/MoS_2 composite coatings under vacuum environment.

it is easy to confirm that the incorporation of Pb into the composite coating is responsible for the long lifetime of coatings.

To obtain the wear mechanism of Pb-Ti/MoS_2 composite coatings under vacuum condition, the corresponding optical images of the wear tracks after 20,000 sliding cycles are shown in Fig. 13. A similar phenomenon to high RH condition (Fig. 8) can be observed that some grooves are seen on the track regions. This is because a bit of wear debris embed in the surface of the steel ball and act as fixed indenters, generating many fine parallel grooves in the sample surface [48]. Moreover, with the increasing Pb content, the width of wear track and quantity of groove decrease gradually. Noticeably, as the Pb content rises to 4.6 at.% (Run No. 3 coating), the wear track is more shallow and narrow than other coatings and the ploughing wear effect is not obvious, which is attributed to a relative dense structure of coating. Beyond of this threshold value of 4.6 at.% Pb, the excessive Pb atoms in turn cause the structure deterioration and lead to the decrease of wear resistance of coating, thus increasing the width of wear track and quantity of groove. Similar results can be found in other study of single-doped MoS_2 coatings such as Au [25], Ti [32] and Cr [26] that the optimal concentration of metal-doping can achieve optimal mechanical and tribological performance.

As mentioned above, the excellent tribological performance of Pb-Ti/MoS_2 composite coatings in both humid and vacuum environments is closely related to the mechanical properties. The classical theories that emphasise hardness as the prime property to define the wear resistance of a coating shall not be pursued, since this will restrict the practical applicability of such coatings [49]. For instance, the Run No. 2 coating has the highest hardness while the tribological performance is not optimal ones. According to the Leyland's opinion [50], high *H/E* ratio is often as a reliable indicator of good wear resistance for a coating. Therefore, the wear resistance of a coating can be improved by achieving a high *H/E* value. To further explore the relationship between the tribological performance and mechanical property of the coatings, the ratios of hardness to elastic modulus (*H/E*) for the Ti/MoS_2 and Pb-Ti/MoS_2 composite coatings as a function of the Pb content are calculated and given in Fig. 14. For the Ti/MoS_2 coating, the *H/E* value is lowest in all tested coatings. Relatively low levels of co-doping metal (2.0–2.9 at.% Ti, 4.6–6.3 at.% Pb) lead to a significant increase in the values of *H/E*. And a maximum *H/E* value about 0.079 is obtained for the composite coatings with 4.6 at.% of Pb. Then the *H/E* values decrease rapidly with further increasing Pb content. Accordingly, we can safety conclude that the mechanical property of the coatings plays a vital role in the tribological performance of Pb-Ti/MoS_2 composite coatings.

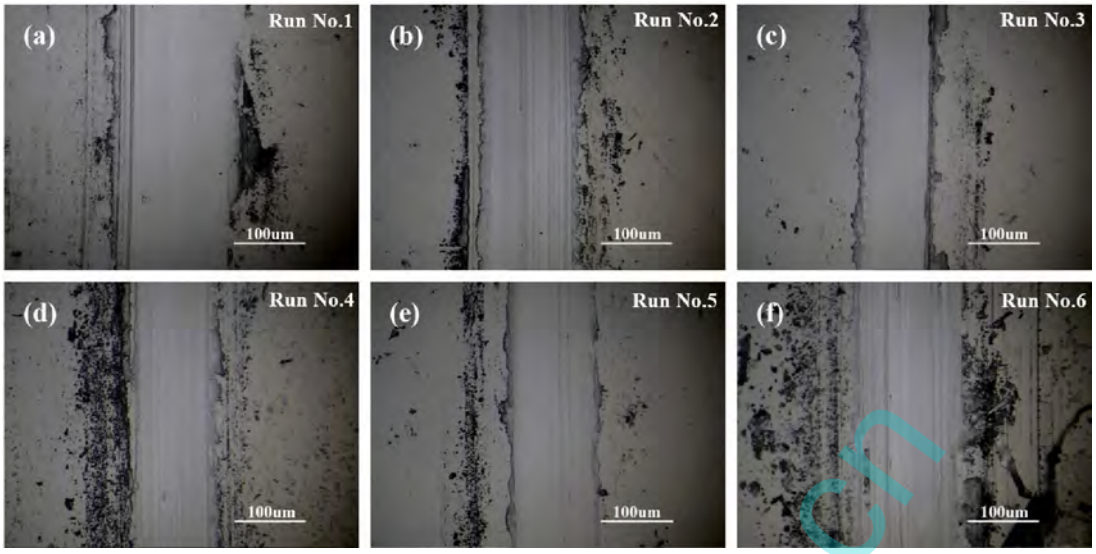

Fig. 13. Optical images of wear tracks of the Ti/MoS_2 and Pb-Ti/MoS_2 composite coatings after 20,000 sliding cycles under vacuum.

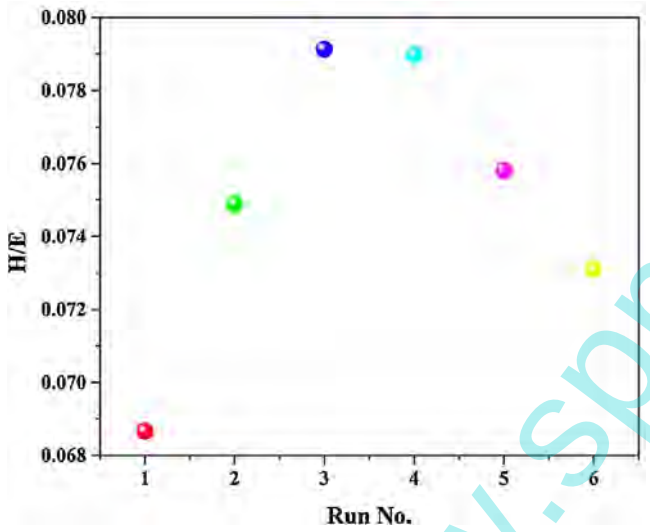

Fig. 14. *H/E* value of Ti/MoS_2 and Pb-Ti/MoS_2 composite coatings.

4. Conclusions

In summary, we had synthesized Pb-Ti co-doped MoS_2 coatings by unbalanced magnetron sputtering system, and discussed the relationship of microstructure and mechanical properties with Pb content. It was demonstrated that the roughness of Pb-Ti/MoS_2 composite coatings decreased with the increase in the Pb content, and the hardness and elastic modulus decreased first and increased afterwards with the increasing Pb content. The findings indicated that the mechanical properties of Pb-Ti/MoS_2 composite coatings were better than the Ti/MoS_2 composite coatings, which is attributed to a transformation that the microstructure of coatings changes from the porous columnar structure for Ti/MoS_2 composite coating to the dense amorphous structure for Pb-Ti/MoS_2 composite coating. Furthermore, the Pb-Ti/MoS_2 composite coatings exhibit excellent self-adaptivity in both of humid environment and vacuum condition. The Pb-Ti/MoS_2 composite coatings with optimal tribological performance were the coating containing about 6.3 at.% Pb in humid environment and 4.6 at.% Pb in vacuum, depending on the higher value of H/E for these two contents. Specifically, the ultra-low friction coefficient with a minimum value of 0.006 under the vacuum condition can be achieved for Pb-Ti/MoS_2 composite coating containing about 4.6 at.% Pb. More importantly, a series of Pb-Ti/MoS_2 coatings with slight Pb will be expected to produce more valuable coatings for possible applications. Hence, multi-metal doping is a promising approach to design the MoS_2 coatings as the environmentally adaptive lubricants.

Acknowledgements

The authors are grateful for financial support from the National Key Basic Research Program (No.2014CB643302), the National Natural Science Foundation of China (No.41506098), and the Strategic Leading Science & Technology Programme (XDA13040600).

References

[1] L. Rapoport, Y. Bilik, Hollow Nanoparticles of WS_2 as Potential Solid-StateLubricants, Nature 387 (1997) 791–793.
[2] M. Chhowalla, G.A.J. Amaratunga, Thin films of fullerene-like MoS_2 nanoparticles with ultra-low friction and wear, Nature 407 (2000) 164–167.
[3] W.X. Chen, J.P. Tu, Z.D. Xu, R. Tenne, R. Rosenstveig, W.L. Chen, H.Y. Gan, Wear and friction of Ni-P electroless composite coating including inorganic fullerene-WS_2 nanoparticles, Adv. Eng. Mater. 4 (2002) 686–690.
[4] T.W. Scharf, S.V. Prasad, M.T. Dugger, P.G. Kotula, R.S. Goeke, R.K. Grubbs, Growth, structure, and tribological behavior of atomic layer-deposited tungsten disulphide solid lubricant coatings with applications to MEMS, Acta Mater. 54 (2006) 4731–4743.
[5] T.W. Scharf, P.G. Kotula, S.V. Prasad, Friction and wear mechanisms in MoS_2/Sb_2O_3/Au nanocomposite coatings, Acta Mater. 58 (2010) 4100–4109.
[6] D.G. Teer, New solid lubricant coatings, Wear 251 (2001) 1068–1074.
[7] B. Weng, X. Zhang, N. Zhang, Z.R. Tang, Y.J. Xu, Two-dimensional MoS_2 nanosheet-coated Bi_2S_3 discoids: synthesis, formation mechanism, and photocatalytic application, Langmuir 31 (2015) 4314–4322.
[8] T. Polcar, A. Cavaleiro, Review on self-lubricant transition metal dichalcogenide nanocomposite coatings alloyed with carbon, Surf. Coat. Technol. 206 (2011) 686–695.
[9] S. Domiínguez-Meister, M. Conte, A. Igartua, R.C. Rojas, J.C. Sánchez-López, Self-lubricity of WSe_x nanocomposite coatings, ACS Appl. Mater. Interfaces 7 (2015) 7979–7986.
[10] A.A. Voevodin, T.A. Fitz, J.J. Hu, J.S. Zabinski, Nanocomposite tribological coatings with chameleon surface adaptation, J. Vac. Sci. Technol. A 20 (2002) 1434–1444.
[11] R.I. Christy, H.R. Ludwig, Rf sputtered MoS_2 parameter effects on wear life, Thin Solid Films 64 (1979) 223–229.
[12] X. Zhang, R.G. Vitchev, W. Lauwerens, L. Stals, J. He, J.P. Celis, Effect of crystallographic orientation on fretting wear behaviour of MoS_x coatings in dry and humid air, Thin Solid Films 396 (2001) 69–77.
[13] P.D. Fleischauer, Effects of crystallite orientation on environmental stability and lubrication properties of sputtered MoS_2 thin films, ASLE Trans. 27 (1984) 82–88.

[14] D.G. Teer, J. Hampshire, V. Fox, V. Bellido-Gonzalez, The tribological properties of MoS_2/metal composite coatings deposited by closed field magnetron sputtering, Surf. Coat. Technol. 94 (1997) 572–577.
[15] M.R. Hilton, R. Bauer, S.V. Didziulis, M.T. Dugger, J.M. Keem, J. Scholhamer, Structural and tribological studies of MoS_2 solid lubricant films having tailored metal-multilayer nanostructures, Surf. Coat. Technol. 53 (1992) 13–23.
[16] L.E. Seitzman, R.N. Bolster, I.L. Singer, Effects of temperature and ion-to-atom ratio on the orientation of IBAD MoS_2 coatings, Thin Solid Films 260 (1995) 143–147.
[17] N.M. Renevier, H. Oosterling, U. König, H. Dautzenberg, B.J. Kim, L. Geppert, J. Leopold, Performance and limitations of MoS_2/Ti composite coated inserts, Surf. Coat. Technol. 172 (2003) 13–23.
[18] H. Singh, K.C. Mutyala, H. Mohseni, T.W. Scharf, R.D. Evans, G.L. Doll, Tribological performance and coating characteristics of sputter-Deposited Ti-Doped MoS_2 in rolling and sliding contact, Tribol. Trans. 58 (2015) 767–777.
[19] K.J. Wahl, L.E. Seitzman, R.N. Bolster, I.L. Singer, Low-friction high-endurance, ion-beam-deposited Pb-Mo-S coatings, Surf. Coat. Technol. 73 (1995) 152–159.
[20] K.J. Wahl, D.N. Dunn, I.L. Singer, Wear behavior of Pb-Mo-S solid lubricating coatings, Wear 230 (1999) 175–183.
[21] S.D. Dvorak, K.J. Wahl, I.L. Singer, In situ analysis of third body contributions to sliding friction of a Pb–Mo–S coating in dry and humid air, Tribol. Lett. 28 (2007) 263–274.
[22] J.J. Nainaparampil, A.R. Phani, J.E. Krzanowski, J.S. Zabinski, Pulsed laser-ablated MoS_2-Al films: friction and wear in humid conditions, Surf. Coat. Technol. 187 (2004) 326–335.
[23] J.D. Holbery, E. Pflueger, A. Savan, Y. Gerbig, Q. Luo, D.B. Lewis, W.D. Munz, Alloying MoS_2 with Al and Au: structure and tribological performance, Surf. Coat. Technol. 169 (2003) 716–720.
[24] S. Mikhailov, A. Savan, E. Pflüger, L. Knoblauch, R. Hauert, M. Simmonds, H. Van Swygenhoven, Morphology and tribological properties of metal (oxide)–MoS_2 nanostructured multilayer coatings, Surf. Coat. Technol. 105 (1998) 175–183.
[25] M.C. Simmonds, A. Savan, E. Pflüger, H. Van Swygenhoven, Mechanical and tribological performance of MoS_2 co-sputtered composites, Surf. Coat. Technol. 126 (2000) 15–24.
[26] X. Ding, X.T. Zeng, X.Y. He, Z. Chen, Tribological properties of Cr-and Ti-doped MoS_2 composite coatings under different humidity atmosphere, Surf. Coat. Technol. 205 (2010) 224–231.
[27] T.W. Scharf, S.V. Prasad, Solid lubricants: a review, J. Mater. Sci. 48 (2013) 511–531.
[28] H. Li, G. Zhang, L. Wang, Low humidity-sensitivity of MoS_2/Pb nanocomposite coatings, Wear 350 (2016) 1–9.
[29] P. Stoyanov, R.R. Chromik, D. Goldbaum, J.R. Lince, X. Zhang, Microtribological performance of Au–MoS_2 and Ti–MoS_2 coatings with varying contact pressure, Tribol. Lett. 40 (2010) 199–211.
[30] H. Li, G. Zhang, L. Wang, The role of tribo-pairs in modifying the tribological behavior of the MoS_2/Ti composite coating, J. Phys. D: Appl. Phys. 49 (2016) 095501.
[31] J. Pu, S. Ren, Z. Lu, L. Wang, A feasible multilayer structure design for solid lubricant coatings in a lunar environment, RSC Adv. 6 (2016) 65504–65517.
[32] X. Qin, P. Ke, A. Wang, K.H. Kim, Microstructure, mechanical and tribological behaviors of MoS_2-Ti composite coatings deposited by a hybrid HIPIMS method, Surf. Coat. Technol. 228 (2013) 275–281.
[33] I. Bertóti, M. Mohai, N.M. Renevier, E. Szilágyi, XPS investigation of ion beam treated MoS_2-Ti composite coatings, Surf. Coat. Technol. 125 (2000) 173–178.
[34] NIST X-ray Photoelectron Spectroscopy Database, Version 3.3, National Institute of Standards and Technology, USA, 2003.
[35] J. Yu, C.Y. Jimmy, B. Cheng, X. Zhao, Photocatalytic activity and characterization of the sol-gel derived Pb-doped TiO_2 thin films, J. Sol-Gel Sci. Technol. 24 (2002) 39–48.
[36] J.R. Lince, M.R. Hilton, A.S. Bommannavar, Metal incorporation in sputter-deposited MoS_2 films studied by extended X-ray absorption fine structure, J. Mater. Res. 10 (1995) 2091–2105.
[37] V. Rigato, G. Maggioni, D. Boscarino, L. Sangaletti, L. Depero, V.C. Fox, D. Teer, C. Santini, A study of the structural and mechanical properties of Ti-MoS_2 coatings deposited by closed field unbalanced magnetron sputter ion plating, Surf. Coat. Technol. 116 (1999) 176–183.
[38] T.J. Wieting, J.L. Verble, Infrared and Raman studies of long-wavelength optical phonons in hexagonal MoS_2, Phys. Rev. B 3 (1971) 4286.
[39] D.Y. Wang, C.L. Chang, Z.Y. Chen, W.Y. Ho, Microstructural and tribological characterization of MoS_2-Ti composite solid lubricating films, Surf. Coat. Technol. 120 (1999) 629–635.
[40] J. Moser, H. Liao, F. Levy, Texture characterisation of sputtered MoS_2 thin films by cross-sectional TEM analysis, J. Phys. D: Appl. Phys. 23 (1990) 624.
[41] T. Moskalewicz, S. Zimowski, B. Wendler, P. Nolbrzak, A. Czyrska-Filemonowicz, Microstructure and tribological properties of low-friction composite MoS_2 (Ti, W) coating on the oxygen hardened Ti-6Al-4 V alloy, Met. Mater. Int. 20 (2014) 269–276.
[42] E. Bauer, Epitaxy of metals on metals, Application of Surface Science 11 (1982) 479–494.
[43] E. Martinez, R. Sanjines, A. Karimi, J. Esteve, F. Lévy, Mechanical properties of nanocomposite and multilayered Cr-Si-N sputtered thin films, Surf. Coat. Technol. 180 (2004) 570–574.
[44] A.H. Chokshi, A. Rosen, J. Karch, H. Gleiter, On the validity of the Hall-Petch relationship in nanocrystalline materials, Scr. Metall. 23 (1989) 1679–1683.
[45] H.S. Myung, H.M. Lee, L.R. Shaginyan, J.G. Han, Microstructure and mechanical properties of Cu doped TiN superhard nanocomposite coatings, Surf. Coat. Technol. 163 (2003) 591–596.
[46] J.L. He, Y. Setsuhara, I. Shimizu, S. Miyake, Structure refinement and hardness enhancement of titanium nitride films by addition of copper, Surf. Coat. Technol. 137 (2001) 38–42.
[47] C.Y.H. Lim, D.K. Leo, J.J.S. Ang, M. Gupta, Wear of magnesium composites reinforced with nano-sized alumina particulates, Wear 259 (2005) 620–625.
[48] R.I. Trezona, D.N. Allsopp, I.M. Hutchings, Transitions between two-body and three-body abrasive wear: influence of test conditions in the microscale abrasive wear test, Wear 225 (1999) 205–214.
[49] J.F. Archard, Contact and rubbing of flat surfaces, J. Appl. Phys. 24 (1953) 981.
[50] A. Leyland, A. Matthews, On the significance of the H/E ratio in wear control: a nanocomposite coating approach to optimised tribological behaviour, Wear 246 (2000) 1–11.